Dendritic Assembly of Gold Nanoparticles during Fuel-Forming Electrocatalysis

Karthish Manthiram,[†,§,∥] Yogesh Surendranath,[‡,§,⊥,∥] and A. Paul Alivisatos*[,‡,§,∥]

[†]Department of Chemical and Biomolecular Engineering, [‡]Department of Chemistry, [§]Kavli Energy Nanosciences Institute, and [⊥]Miller Institute for Basic Research in Science, University of California, Berkeley, California 94720, United States

[∥]Materials Sciences Division, Lawrence Berkeley National Laboratory, Berkeley, California 94720, United States

S *Supporting Information*

ABSTRACT: We observe the dendritic assembly of alkanethiol-capped gold nanoparticles on a glassy carbon support during electrochemical reduction of protons and CO_2. We find that the primary mechanism by which surfactant-ligated gold nanoparticles lose surface area is by taking a random walk along the support, colliding with their neighbors, and fusing to form dendrites, a type of fractal aggregate. A random walk model reproduces the fractal dimensionality of the dendrites observed experimentally. The rate at which the dendrites form is strongly dependent on the solubility of the surfactant in the electrochemical double layer under the conditions of electrolysis. Since alkanethiolate surfactants reductively desorb at potentials close to the onset of CO_2 reduction, they do not poison the catalytic activity of the gold nanoparticles. Although catalyst mobility is typically thought to be limited for room-temperature electrochemistry, our results demonstrate that nanoparticle mobility is significant under conditions at which they electrochemically catalyze gas evolution, even in the presence of a high surface area carbon and binder. A careful understanding of the electrolyte- and polarization-dependent nanoparticle aggregation kinetics informs strategies for maintaining catalyst dispersion during fuel-forming electrocatalysis.

Critical catalytic transformations, such as the electrochemical reduction of carbon dioxide, require the development of high surface area catalysts that maintain their dispersion over time. Practical electrocatalysts typically consist of nanoscale crystallites, which provide high surface-area-to-volume ratios and can be easily incorporated into membrane electrode assemblies.[1] Nanocrystalline catalysts also exhibit unique electronic and surface structures compared to their bulk counterparts.[2] However, highly dispersed nanocrystals are thermodynamically unstable relative to their corresponding bulk crystalline phase because of the high degree of coordinative unsaturation of their surface atoms. This provides a strong driving force for reducing catalyst dispersion, which occurs via two principal mechanisms: (1) diffusion of atomic species between nanoparticles, commonly referred to as Ostwald ripening,[3] or (2) diffusion, collision, and coalescence of entire nanoparticles.[4] Limiting these two transport processes is critical for maintaining high catalyst dispersion and preserving high activity per unit mass of the material.

Noble metals, such as gold, are attractive for electrocatalysis because they exhibit increased resistance to Ostwald ripening compared to other metals.[5] Gold, in the form of foils,[6,7] nanoparticles,[8,9] and clusters,[10] is a selective catalyst for reducing CO_2 to CO. For gold under reducing conditions, the primary mechanism available for surface area loss is the diffusion and fusion of entire nanoparticles. At elevated temperature, successive diffusion of individual atoms along the surface of the nanoparticle collectively leads to a random walk of the entire nanoparticle along the support. At room temperature, though, there is insufficient thermal energy to drive such a process for gold.[11,12] Despite this, we find that during the electrochemical reduction of protons and CO_2, a gold nanoparticle electrocatalyst takes a random walk along the support, fuses with its neighbors, and forms dendrites.

As a model catalytic system, we use gold nanoparticles supported on glassy carbon to electrochemically reduce CO_2. Dodecanethiol-capped gold nanoparticles[13] of diameter 4.2 ± 0.5 nm were spin-coated onto a glassy carbon plate (Supporting Information (SI)). This deposition method gives rise to a random array of individual gold nanoparticles at an areal density of ~3 × 10^{11} particles/cm^2 (Figure 1A). Gold nanoparticle-coated glassy carbon plates prepared in this fashion served as the working electrode in a three-electrode electrochemical cell containing saturated CO_2/0.1 M $NaHCO_3$ electrolyte (hereafter referred to as 0.1 M $NaHCO_3$ buffer) (SI). Experiments were conducted potentiostatically by polarizing to a desired potential and measuring the current versus time (Figures S1). All potentials are reported versus the reversible hydrogen electrode. Alkanethiols are a convenient ligand for synthesizing gold nanoparticles[14] but are generally thought to poison catalytic sites by blocking access to reactants.[15] The thiol is not a poison for electrochemical CO_2 reduction because it is desorbed from the gold surface at potentials at which we observe appreciable current densities. Indeed, we observe comparable current densities for CO_2 reduction on our gold nanoparticle electrodes and gold foils when we normalize for surface area (Figure S3), although the Faradaic efficiency for CO_2 reduction to CO is lower for our dodecanethiol-capped gold nanoparticle electrodes (SI).

Upon polarization at −1.2 V, small dendrites with an average diameter of 13 nm formed after 10 min (Figure 1B), and even
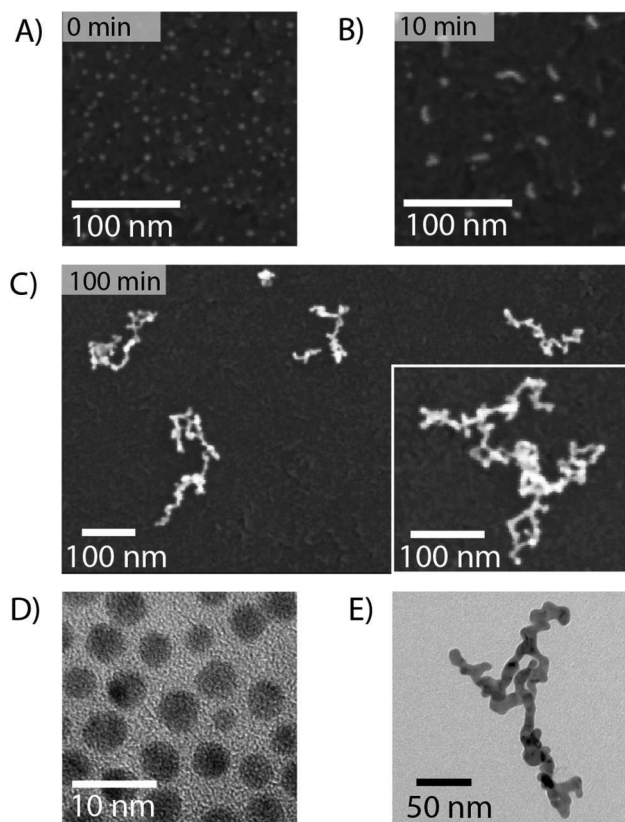
Figure 1. SEM of gold nanoparticles supported on glassy carbon after (A) 0, (B) 10, and (C) 100 min of polarization at −1.2 V in 0.1 M NaHCO$_3$ buffer. TEM of (D) as-synthesized gold nanoparticles and (E) a dendrite formed after 100 min of polarization.

larger dendrites with an average diameter of 140 nm formed after 100 min (Figure 1C) of electrolysis, as found using *ex situ* scanning electron microscopy (SEM). Transmission electron microscopy (TEM) analysis reveals that the initially spherical particles (Figure 1D) fused into branched dendritic structures (Figure 1E).

To further examine the mechanism by which dendrites form, we modeled the diffusion and coalescence of nanoparticles using a random walk algorithm (SI). Simulations of this type are well suited to modeling dendrite formation, as they have been shown to reproduce the patterns that arise from colloid aggregation.[16,17] For each simulation, the initial state consists of a square lattice with periodic boundary conditions that is randomly populated with particles (Figure 2A) at the areal density that we experimentally observe by SEM (SI). In each iteration of the simulation, a randomly chosen particle moves randomly by one unit in any direction. When two particles occupy neighboring sites, they fuse irreversibly to form an aggregate with a probability given by the sticking coefficient p_s, which we briefly assume to be unity. If the system is constrained such that fused particles remain immobile on the substrate, small, unbranched aggregates result from the simulation when no more individual particles remain (Figure 2B). In order to form the larger, highly branched structures observed experimentally (Figure 1C), this constraint must be lifted. When the initially formed aggregates are also allowed to move, much larger dendrites are produced (Figure 2C) if the simulation is allowed to run until the average diameter of the dendrites is equal to that observed experimentally after 100 min of electrolysis (Figure 1C). While this model suggests that
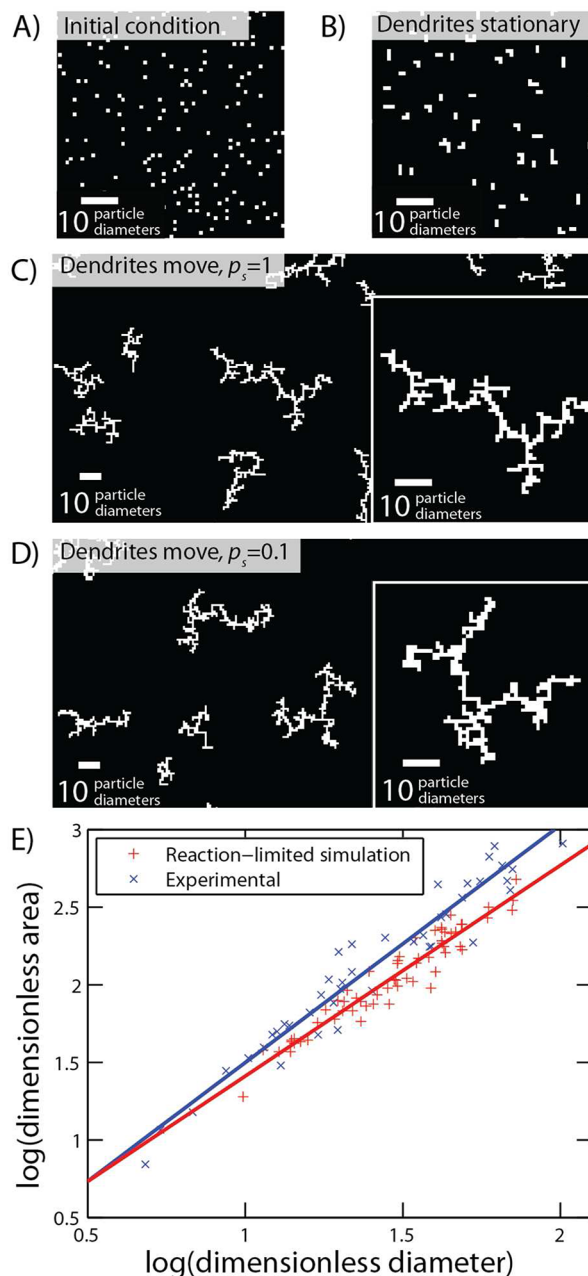

Figure 2. Random walk simulations of dendrite formation. (A) Initial condition. (B) Simulated dendrites if only individual particles move with a sticking coefficient of $p_s = 1$. (C,D) Simulated dendrites if dendrites also move with a sticking coefficient of $p_s = 1$ (C) and 0.1 (D). (E) Dendrite area versus diameter. The solid line indicates a linear fit to the data. The dendrite diameter and area were non-dimensionalized using the particle diameter and square of the particle diameter, respectively.

small aggregates remain mobile over the course of electrolysis, the forces that drive this motion remain unclear. In addition to Brownian motion, bubble formation and particle charging may contribute, particularly at very negative applied potentials.

If we impose a kinetic barrier to particle fusion by decreasing the sticking coefficient to $p_s = 0.1$, we observe that dendrites composed of thicker segments of approximately two initial particle diameters form (Figure 2D), more closely matching the dendrite filament thickness of two to three initial particle diameters obtained experimentally (Figure 1E).

The dendrites formed upon electrolysis can be viewed as fractal structures, which are self-similar on multiple length scales.[18,19] Fractals are characterized by a non-integer dimensionality, which is given by the slope of a linear fit to a plot of the logarithm of the area occupied by a dendrite versus the logarithm of the maximum caliper diameter of the same dendrite (SI). We expect fractal dimensionalities between the Euclidean dimensions of 1 and 2, with larger values denoting more space-filling structures. We first calculate the fractal dimensionality of dendrites produced after 100 min of polarization at −1.2 V. Then, random walk simulations of dendrite formation are allowed to proceed until the average of the maximum caliper diameters of the simulated dendrites is the same as that measured experimentally. Figure 2E plots the logarithm of area versus the logarithm of maximum caliper diameter for experimental and simulated dendrites. Both sets of dendrites span a similar range and display a roughly linear trend. The fractal dimensionality of the experimentally produced dendrites is 1.5 ± 0.1, which is comparable to the fractal dimensionalities of 1.4 ± 0.1 and 1.3 ± 0.1 for reaction-limited and diffusion-limited dendrite formation, respectively. This analysis further suggests that a diffusion-collision model is sufficient to describe the pathway for dendrite formation during electrolysis.

The course of dendrite formation is strongly dependent on electrode potential. At −0.2 V, there is no observable dendritic assembly (Figure 3A), and the electrode appears identical to the
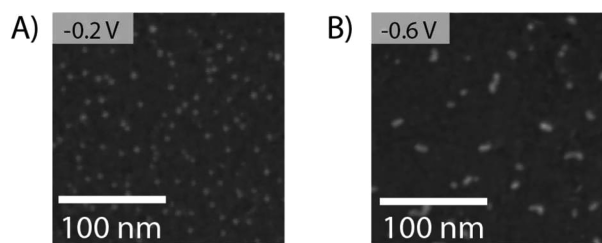

Figure 3. SEMs of electrodes after polarization for 10 min in 0.1 M NaHCO$_3$ buffer at (A) −0.2 and (B) −0.6 V.

unpolarized electrode (Figure 1A). However, dendritic assembly is observed at −0.6 V (Figure 3B) and at more negative potentials (Figure 1B). Importantly, the potential of this transition coincides with the alkanethiolate reductive desorption potential of −0.6 V,[20,21] suggesting that productive particle fusion occurs more readily when thiols are no longer chemisorbed to the gold nanoparticle surface.

Surprisingly, dodecanethiol also influences the nanoparticle assembly behavior well beyond its reductive desorption potential. At potentials beyond −0.6 V, the thiolate−gold chemisorption bond is ruptured; however, the dissociated thiolate may remain physisorbed to the gold surface or carbon support. Indeed, X-ray photoelectron spectroscopy of gold nanoparticle-decorated electrodes subjected to exhaustive polarization beyond −1.2 V reveals that thiolates remain on the surface (Figures S4 and S5).[22] The degree to which the alkanethiol physisorbs is related to its solubility in the electrolyte, which can be modulated by changing the pH.[20,23] To interrogate the impact of physisorbed ligands, we examined the dendritic assembly in acidic and basic electrolytes under argon gas in the absence of CO$_2$. Although only H$_2$ is evolved under these conditions, the pH dependence of dendritic assembly provides insights into the role of the physisorbed thiolates. There is no observable dendritic assembly in 0.1 M H$_2$SO$_4$, pH 1, but rapid

dendritic assembly is observed during electrolysis in both 0.1 M NaHCO$_3$, pH 6.8, and 0.1 M KOH, pH 12 (Figure 4A,C,E). This
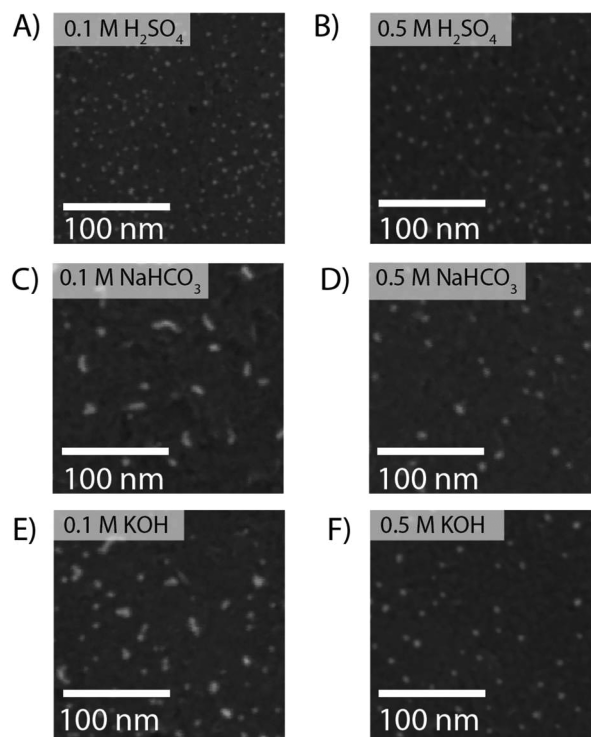

Figure 4. SEMs of electrodes after polarization at −1.2 V for 10 min in (A) 0.1 M H$_2$SO$_4$, (B) 0.5 M H$_2$SO$_4$, (C) 0.1 M NaHCO$_3$, (D) 0.5 M NaHCO$_3$, (E) 0.1 M KOH, and (F) 0.5 M KOH.

pH dependence is in line with the significantly higher solubility of dodecanethiolate relative to dodecanethiol in aqueous electrolytes.[24] As dodecanethiol has a pK_a of ∼10.5, reductive desorption is accompanied by protonation to form a surface adsorbed thiol in acidic media. These adsorbed thiols sterically impede productive gold nanoparticle fusion events; thus, the sticking coefficient is sufficiently low such that we observe essentially no dendritic assembly (Figure 4A). In contrast, in alkaline media, in which the thiolate is not protonated upon reductive desorption, there is rapid dendritic assembly (Figure 4E). At a nearly neutral pH of 6.8, the observation of dendritic assembly (Figure 4C) appears contrary to what we would expect on the basis of the thiol pK_a of 10.5; however, under reductive polarization, the electrolyte can become significantly more basic in the vicinity of the electrode, especially in electrolytes with low buffer capacity. We believe that the increased local pH under polarization is responsible for increasing the local solubility of the thiolate and driving dendritic assembly at intermediate pHs. Consistent with this hypothesis, we observe reduced dendritic assembly in 0.5 M NaHCO$_3$ buffer (Figure 4D), in which the increased electrolyte strength diminishes local pH gradients at the electrode surface. Additionally, the increased ionic strength may serve to screen charge−charge repulsion between the physisorbed thiolates, inhibiting their dissociation from the surface.[23] We also observe that dendritic assembly is suppressed upon going from 0.1 to 0.5 M KOH (Figure 4F), suggesting that dielectric screening may also play a role in alkaline media; the reduced dendritic assembly also improves activity for hydrogen evolution (Figure S2). Solubility arguments can also be used to rationalize why dodecanethiol is a more effective ligand for

retarding dendritic assembly relative to dodecylamine (Figure S6). Together, these results indicate that the electrolyte composition is the primary determinant of the rate of dendritic assembly by modulating the solubility of physisorbed surfactants.

The mobility of nanoparticles electrochemically catalyzing gas evolution is a fundamental process that occurs even when the nanoparticles are encapsulated in a binder, as is common in practical catalytic systems. To demonstrate this, we have examined the nanoparticle mobility and fusion events in a composite system comprised of acetylene black and poly-(vinylidene fluoride). In this binder, dendritic assembly still occurred (Figure 5) but at a slower rate than in the absence of
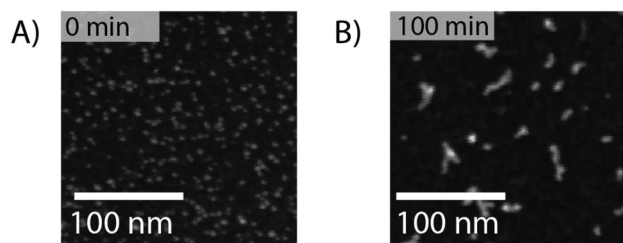

Figure 5. SEM of electrodes consisting of gold nanoparticles, acetylene black, and poly(vinylidene fluoride) (A) prior to polarization and (B) following 100 min of polarization at −1.2 V in 0.1 M $NaHCO_3$ buffer.

these additives. This suggests that the additives simply act to provide steric hindrance between the diffusing particles, thereby reducing the collision frequency. To block the diffusion–aggregation process completely would require that the nanoparticles be bound to the substrate tightly enough to perturb the nanoparticles themselves. What we have found here is that the diffusion–aggregation process can be controlled by tuning the ligand chemistry in such a way as to allow aggregation to proceed up to a point, while retaining functional catalytic activity.

Our work demonstrates that carbon-supported nanoparticles are subject to diffusion, collision, and fusion to form dendritic assemblies under reductive polarization, even at room temperature and in the presence of a high surface area carbon and binder. A simple random walk model is sufficient to describe the formation of dendrites with agreement between the simulated and experimental fractal dimensionalities. Additionally, this study highlights the critical role of electrolyte- and polarization-dependent surface chemistry in mediating nanoparticle aggregation during electrocatalysis. By giving an improved understanding of the mechanism by which gold nanoparticles lose surface area via dendritic assembly, these studies inform strategies for preserving catalyst dispersion in order to maintain activity under harsh electrochemical conditions.

ASSOCIATED CONTENT

Ⓢ Supporting Information

Experimental and simulation methods, X-ray photoelectron spectra, electrochemical data, and additional scanning electron micrographs. This material is available free of charge via the Internet at http://pubs.acs.org.

AUTHOR INFORMATION

Corresponding Author

alivis@berkeley.edu

Notes

The authors declare no competing financial interest.

REFERENCES

(1) Weidner, J. W.; Sethuraman, V. A.; Van Zee, J. W. *Interface* **2003**, *12*, 40.
(2) *Catalysis and Electrocatalysis at Nanoparticle Surfaces*; Wieckowski, A., Savinova, E. R., Vayenas, C. G., Eds.; Marcel Dekker: New York, 2003.
(3) Ostwald, W. *Z. Phys. Chem.* **1900**, *34*, 495.
(4) Smoluchowski, M. *Z. Phys. Chem.* **1917**, *1210*, 129.
(5) Pourbaix, M. *Atlas of Electrochemical Equilibria in Aqueous Solutions*, 2nd ed.; National Association of Corrosion Engineers: Houston, TX, 1974; pp 399−405.
(6) Hori, Y.; Kikuchi, K.; Suzuki, S. *Chem. Lett.* **1985**, *11*, 1695.
(7) Hori, Y. In *Modern Aspects of Electrochemistry*; Vayenas, C. G., White, R. E., Gamboa-Aldeco, M. E., Eds.; Springer: New York, 2008; pp 89−189.
(8) Zhu, W.; Michalsky, R.; Metin, O.; Lv, H.; Guo, S.; Wright, C. J.; Sun, X.; Peterson, A. A.; Sun, S. *J. Am. Chem. Soc.* **2013**, *135*, 16833.
(9) Chen, Y.; Li, C. W.; Kanan, M. W. *J. Am. Chem. Soc.* **2012**, *134*, 19969.
(10) Kauffman, D. R.; Alfonso, D.; Matranga, C.; Qian, H.; Jin, R. *J. Am. Chem. Soc.* **2012**, *134*, 10237.
(11) Wynblatt, P.; Gjostein, N. *Prog. Solid State Chem.* **1975**, *9*, 21.
(12) Baker, R. *J. Catal.* **1982**, *78*, 473.
(13) Hussain, I.; Graham, S.; Wang, Z.; Tan, B.; Sherrington, D. C.; Rannard, S. P.; Cooper, A. I.; Brust, M. *J. Am. Chem. Soc.* **2005**, *127*, 16398.
(14) Brust, M.; Walker, M.; Bethell, D.; Schiffrin, D. J.; Whyman, R. *J. Chem. Soc., Chem. Commun.* **1994**, *7*, 801.
(15) Oudar, J. *Catal. Rev. Eng.* **1980**, *22*, 37.
(16) Witten, T.; Sander, L. *Phys. Rev. Lett.* **1981**, *47*, 1400.
(17) Meakin, P. *Phys. Rev. Lett.* **1983**, *51*, 1119.
(18) Mandelbrot, B. B. *The Fractal Geometry of Nature*; W. H. Freeman and Co.: New York, 1982.
(19) Meakin, P. *Annu. Rev. Phys. Chem.* **1988**, *39*, 237.
(20) Yang, D.; Wilde, C.; Morin, M. *Langmuir* **1996**, *12*, 6570.
(21) Widrig, C.; Chung, C.; Porter, M. *J. Electroanal. Chem.* **1991**, *310*, 335.
(22) Byloos, M.; Al-Maznai, H.; Morin, M. *J. Phys. Chem. B* **1999**, 6554.
(23) Yabroff, D. *Ind. Eng. Chem.* **1940**, *32*, 257.
(24) Emmet, E. E. *Organic Chemistry of Bivalent Sulphur*; Chemical Publishing Co.: New York, 1958.